

Dirac versus Weyl Fermions in Topological Insulators: Adler-Bell-Jackiw Anomaly in Transport Phenomena

Heon-Jung Kim,^{1,*} Ki-Seok Kim,^{2,3,†} J.-F. Wang,⁴ M. Sasaki,⁵ N. Satoh,⁶ A. Ohnishi,⁵ M. Kitaura,⁵ M. Yang,⁴ and L. Li⁴

¹*Department of Physics, College of Natural Science, Daegu University, Gyeongsbuk 712-714, Korea*

²*Department of Physics, Pohang University of Science and Technology (POSTECH), Pohang, Gyeongsbuk 790-784, Korea*

³*Institute of Edge of Theoretical Science (IES),*

Hogil Kim Memorial Building, 5th floor, POSTECH, Pohang, Gyeongsbuk 790-784, Korea

⁴*Wuhan National High Magnetic Field Center, Huazhong University of Science and Technology, Wuhan 430074, China*

⁵*Department of Physics, Faculty of Science, Yamagata University, Kojirakawa, Yamagata 990-8560, Japan*

⁶*Department of Electronics and Computer Science, Iwaki Meisei University, Iwaki, Fukushima 970-8551, Japan*

(Received 28 July 2013; published 10 December 2013)

Dirac metals (gapless semiconductors) are believed to turn into Weyl metals when perturbations, which break either time reversal symmetry or inversion symmetry, are employed. However, no experimental evidence has been reported for the existence of Weyl fermions in three dimensions. Applying magnetic fields near the topological phase transition from a topological insulator to a band insulator in $\text{Bi}_{1-x}\text{Sb}_x$ we observe not only the weak antilocalization phenomenon in magnetoconductivity near zero magnetic fields ($B < 0.4$ T), but also its upturn above 0.4 T *only* for $E//B$. This “incompatible” coexistence between weak antilocalization and “negative” magnetoresistivity is attributed to the Adler-Bell-Jackiw anomaly (“topological” $E \cdot B$ term) in the presence of weak antilocalization corrections.

DOI: [10.1103/PhysRevLett.111.246603](https://doi.org/10.1103/PhysRevLett.111.246603)

PACS numbers: 72.90.+y, 72.10.-d, 72.15.Qm

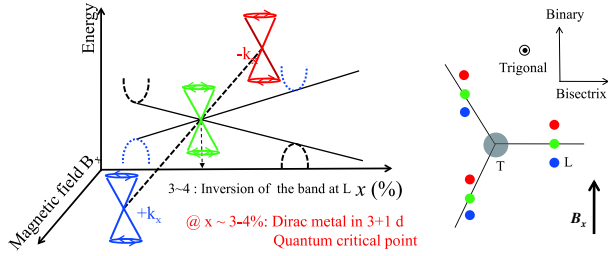
It is rare to observe Weyl fermions in three-dimensional (3D) condensed matter systems. Graphene may be one of the well-studied systems as a two-dimensional (2D) Weyl metallic state, where two types of Weyl fermions with opposite chirality appear at separate momenta [1]. However, no experimental evidence has been reported for the Weyl metallic phase in three dimensions, where they are combined more often to form Dirac fermions. Rigorously speaking, this phenomenon is attributed to the fact that the Dirac spinor is the irreducible representation of the Lorentz group in three dimensions while it is the Weyl spinor in two dimensions [2]. Recently, it has been shown that such a Weyl metallic phase must exist near the topological phase transition from a band insulator to a topological insulator in 3D when either time reversal symmetry or inversion symmetry is not preserved at the critical point [3–7]. Actually, the emergence of Weyl fermions has been claimed long before when magnetic fields are applied to gapless semi-conductors (Dirac metals) [8,9]. A Dirac point is separated into two Weyl points with opposite chirality in momentum space, where their distance is proportional to the applied magnetic field.

The characteristic feature of a Weyl metallic phase is that a Weyl fermion state at one Weyl point must transfer to that at the other Weyl point when currents are driven in the same direction as the momentum to connect two paired Weyl points. This phenomenon is referred to as the Adler-Bell-Jackiw anomaly, which means that the chiral current is not conserved [8,9]. This nonlocal (in momentum space), more accurately, topological “constraint” has been suggested to cause anomalous magnetotransport

phenomena in 3D Weyl metals, that is, “negative” magnetoresistivity (MR) when the applied electric field is parallel to the magnetic field. This anomalous longitudinal MR was shown to arise from the suppression of scattering between two Weyl points as the magnetic fields are increased [10,11]. Unfortunately, this Weyl metallic phase has not been confirmed experimentally. In particular, the negative MR (or “positive” magnetoconductivity-MC) has not been observed yet.

In this Letter we present evidence that supports the emergence of the Weyl metallic phase in $\text{Bi}_{1-x}\text{Sb}_x$ near the critical point of the topological phase transition when magnetic fields are applied. The global phase diagram of $\text{Bi}_{1-x}\text{Sb}_x$ is well known [12–14] (Fig. 1(a)). A topological phase transition from a band insulator to a topological insulator occurs at $x \approx 3\%$, where massless Dirac fermions appear near the L point. Therefore, $\text{Bi}_{1-x}\text{Sb}_x$ at $x \approx 3\%$ is identified as a Dirac metal. Applying magnetic fields near this critical point, it is natural to expect the emergence of a Weyl metallic phase, where the single Dirac point splits into two Weyl points with opposite chirality. The structure of the Dirac points and the Weyl points in the reciprocal space is schematically shown in Fig. 1(b). The magnetic field splits the Dirac points into the Weyl points along the direction of the magnetic field, breaking the rotational symmetry.

We verify the emergence of the Weyl metallic phase by measuring the angle dependence of MR, where the angle corresponds to that between applied magnetic and electric fields. In particular, we observe not only the weak antilocalization near zero magnetic fields ($B < 0.4$ T) but also an

(a) Schematic band structure of $\text{Bi}_{1-x}\text{Sb}_x$ near the L point (left) and in the k space (right)

(b) Measurements of anisotropic transport coefficients

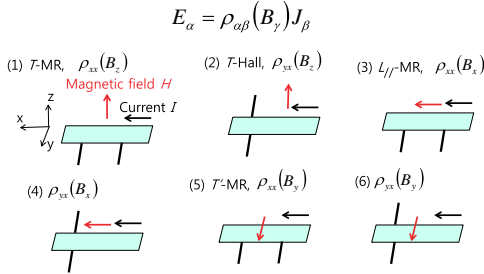


FIG. 1 (color online). (a) A topological phase transition occurs from a band insulator ($x < 3\%$) to a topological insulator ($x > 3\%$) around $x \approx 3\%$, where band touching emerges to form a Dirac cone at the L point. Applying a magnetic field B to this Dirac metal, the Dirac point described by the four-component Dirac spinor is split into two Weyl points described by the two-component Weyl spinors with opposite chirality (red, blue = Weyl, green = Dirac). The distance between these two Weyl points is proportional to B . The right figure depicts the structure of the Dirac points at $B = 0$ and that of the Weyl points at $B \neq 0$ in the reciprocal space, where the Dirac points split along the direction of B . (b) Schematic diagram of the electrical transport measurements.

upturn of or increasing MC above 0.4 T only when both magnetic and electric fields are applied in the same direction. The coexistence between weak antilocalization and negative MR is remarkable. The experimental observation of weak antilocalization corrections is common for systems with strong spin-orbit interactions [15–19]. On the other hand, negative MR results from either weak localization or interaction corrections with diffusive dynamics (diffusive Fermi liquids) [20]. In addition, it can appear when magnetic fluctuations are suppressed via magnetic fields, and thus the corresponding scattering rate decreases [21]. Considering the fact that conventional calculations based on density functional theory describe the band structure of $\text{Bi}_{1-x}\text{Sb}_x$ quite well [12,13], such interaction effects cannot be the physical origin for the negative MR. Then, their coexistence is difficult to understand within the perturbation framework for both nonmagnetic randomness and weak interactions in the presence of spin-orbit scattering.

We attribute the underlying mechanism for the upturn of MC to the Adler-Bell-Jackiw anomaly in the presence of weak antilocalization corrections, comparing experimental

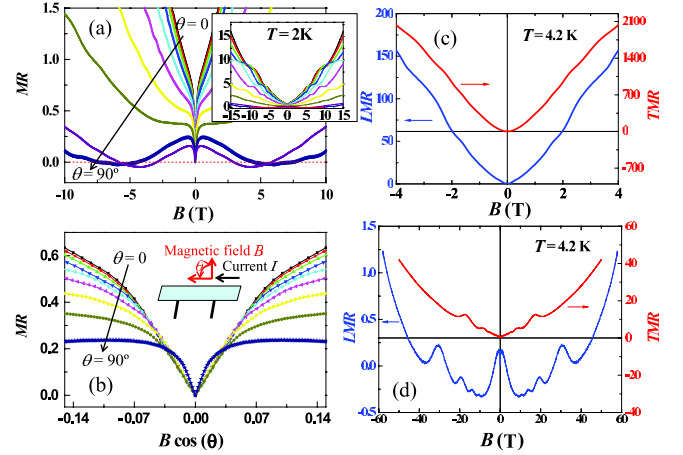


FIG. 2 (color online). (a) Angle-dependent MR. “Negative” MR appears around $\theta = 90^\circ$, which originates from the Adler-Bell-Jackiw anomaly of Weyl fermions. (b) The scaling property of MR in the low-field region. The x axis is the perpendicular field component of $B \cos\theta$. This dip was attributed to the three-dimensional weak antilocalization. (c) Longitudinal and transverse MR for a Bi single crystal. We could not find any negative signals in the longitudinal MR. (d) The transverse and longitudinal MR measured up to 50–60 T in a pulse magnet.

data with theoretical results from the quantum Boltzmann equation approach with the introduction of the topological $E \cdot B$ term [22]. In the “longitudinal” magnetotransport configuration where the electric field is parallel to the magnetic field, the dynamics of Weyl fermions is topologically constrained by the topological $E \cdot B$ term [10,11]. As a result, the MC increases above a critical magnetic field associated with the weak antilocalization. In contrast, only weak antilocalization corrections to the MC were found in the conventional “transverse” magnetotransport measurements, where the magnetic and electric fields were applied in the z and x directions, respectively. This result suggests the unexpected coexistence of weak antilocalization and the upturn of longitudinal MC as the fingerprints of Weyl fermions in three dimensions, which arise from the topological $E \cdot B$ term or the Adler-Bell-Jackiw anomaly.

Figure 1(b) presents a schematic diagram of the experiments for measuring the electrical transport coefficients, $\rho_{\alpha\beta}(B_\gamma)$, which are defined by the equation, $E_\alpha = \rho_{\alpha\beta}(B_\gamma) J_\beta$, where J_β is an electric current of the β direction under a magnetic field B_γ in the γ direction and E_α is the induced electric field in the α direction. The experimental details are explained in Ref. [23].

Figure 2 shows the angle-dependent MR for the configuration and MR up to 60 T at fixed positions, as shown in the schematic diagram, where the configurations for $\theta = 0^\circ$ and 90° were used to measure the transverse [Fig. 1(b)-(1)] and longitudinal [Fig. 1(b)-(3)] MRs, respectively. All the MR data showed a narrow dip below 0.4 T. These dips are similar to those observed in graphene

[16,17] and thin films of 3D topological insulators [18,19], which were attributed to weak antilocalization. On the other hand, an important difference was observed between the previous studies and the present measurements; the weak antilocalization in the data is due to 3D Dirac fermions instead of 2D ones. It is noted that $x \approx 3\%$ corresponds to the critical point, where 3D Dirac fermions appear. One way to confirm the three dimensionality is to determine if the scaling property is satisfied for different angles. If the dynamics of Dirac fermions is 2D, only the magnetic field perpendicular to the plane for the dynamics of such Dirac fermions leads to cyclotron motions. This scaling behavior was not observed in $\text{Bi}_{0.97}\text{Sb}_{0.03}$, supporting the 3D nature of Dirac fermions [Fig. 2(b)]. The MR data will be fitted to the 3D expression for weak antilocalization later.

Unexpected features were noted at higher magnetic fields, particularly for the longitudinal MR configuration of $\theta = 90^\circ$. When θ is near 0° , the MR increased quadratically, indicating the dominance of orbital contributions. This standard behavior changed drastically when θ approached 90° , where the MR decreases considerably just after the dip up to $B \sim 4\text{--}10$ T. Above this field, MR increases again. This negative MR is reproducible. Although different crystals are used, it is observed both in the static and pulsed magnetic fields. On the other hand, we fail to observe such negative signals in pure Bi samples. See Fig. 2(c). In addition, the negative MR was not found deep inside the topological insulating phase, either [23]. Thus, this negative MR is difficult to understand within the perturbation framework incorporating both electronic (magnetic) correlations and nonmagnetic impurities in the presence of spin-orbit interactions. The decrease in longitudinal MR at relatively moderate magnetic fields above the region of weak antilocalization is attributed to the topologically constrained dynamics of Weyl fermions, which is given by the chiral anomaly.

Both $\rho_{xx}(B_z)$ and $\rho_{xx}(B_x)$ are derived based on the quantum Boltzmann equation approach with the introduction of the Adler-Bell-Jackiw anomaly via the semiclassical equations of motion [22,23]. Unfortunately, technical complexity of this methodology does not allow us to have an intuitive physical picture for anomalous behaviors in such transport coefficients. To make the physics more apparent, we also derive these anomalous transport coefficients based on the semiclassical equations of motion only, which is essentially the same as the equation of motion with the Lorentz force for the Hall effect in the elementary solid-state physics except for the introduction of the topological $E \cdot B$ term and the contribution of the Berry curvature. All details are discussed in the Supplemental Material [23] and a recent paper [22].

Disappearance of Weyl fermions with negative chirality gives rise to the production of those with positive chirality, where this dissipationless transfer is equilibrated by several

scattering processes to reach a steady state. The Adler-Bell-Jackiw anomaly and possible scattering channels are described by the semiclassical equation of motion for the momentum, $\dot{\mathbf{p}} = (1 + \frac{e}{c} \mathbf{B} \cdot \boldsymbol{\Omega}_p)^{-1} \{ e \mathbf{E} + \frac{e}{mc} \mathbf{p} \times \mathbf{B} + \frac{e^2}{c} (\mathbf{E} \cdot \mathbf{B}) \boldsymbol{\Omega}_p \} = -\frac{\mathbf{p}}{\tau}$, where τ is an effective mean-free time, determined by the intranode and internode scattering times (node = Weyl point) and $\boldsymbol{\Omega}_p$ is the Berry curvature [23]. Solving this equation of motion to obtain the momentum as a function of both electric and magnetic fields, we find the corresponding electrical current, $\mathbf{J} = ne\dot{\mathbf{r}} = ne(1 + \frac{e}{c} \mathbf{B} \cdot \boldsymbol{\Omega}_p)^{-1} \{ \frac{\mathbf{p}}{m} + e \mathbf{E} \times \boldsymbol{\Omega}_p + \frac{e}{mc} (\boldsymbol{\Omega}_p \cdot \mathbf{p}) \mathbf{B} \}$, where the solution of the velocity was utilized from the other semiclassical equations of motion [23]. It is essential to notice that there are two additional contributions for electric currents other than the conventional term proportional to the momentum, nonzero only when the Berry curvature exists [24,25].

After several straightforward steps with the condition for the Hall effect, $J_y = 0$, we find the expression of $\sigma_L(\mathbf{B}) = (1 + C_W B^2) \cdot \sigma_{WAL} + \sigma_n$ for the longitudinal MC in the weak field region, essentially the same as that from the quantum Boltzmann equation approach, where σ_{WAL} is the conductivity from weak antilocalization corrections associated with intranode scattering and σ_n is that from conventional Fermi surface contributions other than the L -point ‘‘Dirac’’ cone [23]. The most important feature is that the longitudinal MC contains an overall factor of $C_W B^2$ with a positive constant C_W , originating from the topological $E \cdot B$ term. Such a topological term turns out to cause an additional contribution for the z -directional momentum, driven by the x -directional electric field along with the x -directional magnetic field under the influence of Berry curvature [23]. Combined with the last term in the expression of the current, this contribution gives rise to the overall factor proportional to B^2 , which enhances the longitudinal conductivity due to the momentum transfer proportional to the applied magnetic field. In contrast, the transverse MC is expressed by $\sigma_T(\mathbf{B}) = \sigma_{WAL} + \sigma_n$ without the anomaly contribution because the contribution from $E \cdot B$ vanishes. σ_{WAL} and σ_n are additive because they originate from different bands [26]. Considering that σ_n would be determined by residual charge carriers around the T point in momentum space, the conventional Fermi-liquid form $\sigma_n^{-1} = \rho_0 + A \cdot B^2$ is assumed. Recalling the scaling result for the angle dependence of MR, the 3D weak antilocalization formula, given by $\sigma_{WAL} = \Delta \sigma_{WAL} + \sigma_0 = a\sqrt{B} + \sigma_0$, where a and σ_0 are determined from the line of best fit, is used [27].

Figures 3(a) and 3(b) show the transverse MC $\sigma_T(\mathbf{B})$ and longitudinal MC $\sigma_L(\mathbf{B})$, respectively, where the black circles represent the experimental data and the red lines show the theoretical fitting based on the above equations. The essential features of the transverse MC, such as the sharp peak in the zero field region and the gradual decrease up to 1.2 T are reproduced quite well with parameters of

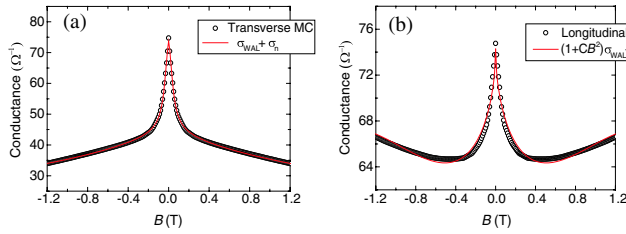


FIG. 3 (color online). (a) Transverse magnetoconductance. The black circles represent the experimental data and the red lines express the theoretical fitting, where both weak antilocalization corrections and normal contributions from other bands are considered. (b) Longitudinal magnetoconductance. The overall factor $C_W B^2$ in front of weak antilocalization corrections is the key feature, which originates solely from the topological $E \cdot B$ term in both the quantum Boltzmann equation and the equation of motion approaches. This is the fingerprint of the Weyl metallic state.

$a = -14.3 \Omega^{-1} T^{-0.5}$, $\sigma_0 = 49.6 \Omega^{-1}$, $\rho_0 = 4.15 \times 10^{-2} \Omega$, and $A = 21.8 \Omega T^{-2}$. We restrict the region of our fitting with $-1.2 \text{ T} < B < 1.2 \text{ T}$ to compare this analysis with the case of the longitudinal MC, where this formula is derived in the weak field region. This successful fitting confirms that the origin of the sharp peak is the 3D weak antilocalization. Similarly, the peak in the zero field region and the upturn of the longitudinal MC are also reproduced well with a reasonable set of parameters of $a = -20.6 \Omega^{-1} T^{-0.5}$, $\sigma_0 = 36.6 \Omega^{-1}$, $\rho_0 = 2.65 \times 10^{-2} \Omega$, $A = 7.3 \times 10^{-3} \Omega T^{-2}$, and $C_W = 1.27 T^{-2}$. All parameters of a , σ_0 , and ρ_0 have similar values for both cases, whereas the value of A in the longitudinal MC is much smaller than that in the transverse MC. This is consistent with our expectation, where the coefficient of the B^2 term in the normal conductivity from the bands around the T point should vanish because there cannot be any orbital motion in the longitudinal MC setup. The upturn of the longitudinal MC above 0.4 T cannot be captured without the correction term of $C_W B^2$, suggesting that the origin of this enhancement is purely topological, i.e., the chiral anomaly in the dynamics of Weyl fermions.

The positive component of the longitudinal MC disappears eventually at the critical magnetic field of $B \sim 4 \text{ T}$ and the MC decreases with increasing B above 4 T. This “reentrant” downturn of MC may be discussed based on the “pair-annihilation” scenario [23]. However, it may be unrealistic to consider such paired Weyl points to move all over the whole Brillouin zone away from the L point, because the band gap is rather large for the wave vectors away from the L point. Although our experiments are in the semiclassical regime associated with the Adler-Bell-Jackiw anomaly [24], it is difficult to exclude the possibility for the formation of Landau levels, increasing magnetic fields to reach the “intermediate” region of the reentrant downturn behavior. It is interesting to observe pronounced oscillations at higher magnetic fields in the

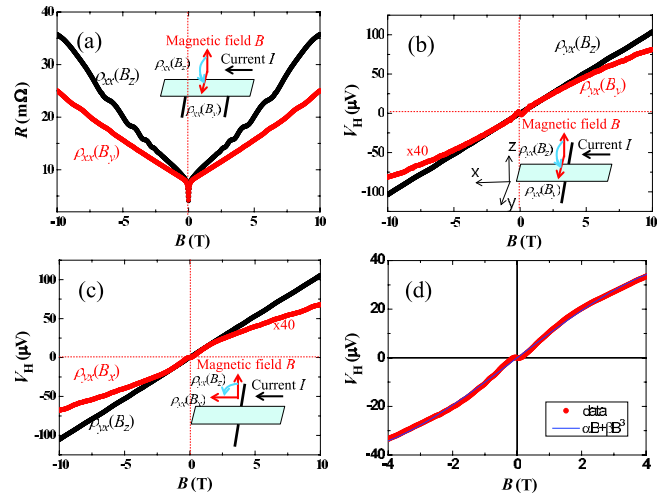


FIG. 4 (color online). (a) Magnetoresistance of $\rho_{xx}(B_z)$ and $\rho_{xx}(B_y)$. (b) The $\rho_{yx}(B_z)$ and $\rho_{yx}(B_x)$ are compared. (c) Comparison of $\rho_{yx}(B_z)$ and $\rho_{yx}(B_x)$. The signal in the latter coefficient is nonzero because of the topological Hall effect, which results from the topological $E \cdot B$ term. This topological Hall effect is regarded as another signature for the Weyl fermions. (d) Transport coefficient $\rho_{yx}(B_x)$ with the theoretical fitting based on the formula $a \cdot B + b \cdot B^3$.

“longitudinal” configuration [Fig. 2(d)], where the cyclotron motion is not possible. In particular, we point out that such quantum oscillations seem to start from the minimum point of the longitudinal MR, implying that the disappearance of the negative MR is correlated with the appearance of pronounced quantum oscillations. The problem on the crossover from the semiclassical to quantum regimes is beyond the scope of the present investigation, which needs to be examined more sincerely near future.

The topological nature of the Weyl metallic state is also manifested in the unconventional transport coefficients. Figure 4 shows the results of the in-plane transverse MR $\rho_{xx}(B_y)$ [Fig. 1(b)-(5)], $\rho_{yx}(B_x)$ [Fig. 1(b)-(4)], and $\rho_{yx}(B_y)$ [Fig. 1(b)-(6)] together with the transverse MR $\rho_{xx}(B_z)$ [Fig. 1(b)-(1)] and $\rho_{yx}(B_z)$ [Fig. 1(b)-(2)]. Of the most notable feature in Fig. 4 is the B dependence of $\rho_{yx}(B_x)$ with reproducible B -linear and B -cubic contributions. Our theoretical approaches reveal that such a nonlinear signal is purely topological in its origin and is given by $\rho_{yx}(B_x) = (1/nec)(\alpha B_x + \beta B_x^3)$ in the weak-field limit, where α and β are constants [23]. According to our theoretical analysis, this is a kind of the Hall effect, which originates from 3D Weyl fermions. Effective Lorentz forces due to the Berry curvature and the topological $E \cdot B$ term cause the y -directional electric fields, which lead eventually to the B -linear and the B -cubic contributions, respectively. In this respect we call it topological Hall effect. Figure 4(d) shows the fit of the $\rho_{yx}(B_x)$ data in the region for $-4 \text{ T} < B < 4 \text{ T}$ to the formula of $aB + bB^3$, where a and b were found to be positive and negative, respectively. This formula fits

the $\rho_{yx}(B_x)$ data quite well except for the zero-field region. Another important experimental finding is nonlinearity in the conventional Hall resistivity [$\rho_{yx}(B_z)$] near the zero magnetic field. This is thought to be the anomalous Hall signal of the 3D Weyl fermions, which should be distinguished from the 2D case [28,29].

Finally, we remark two different regimes for the Adler-Bell-Jackiw anomaly. The present analysis of the semiclassical regime is justified when the chemical potential is much larger than the cyclotron frequency. On the other hand, the so-called ultraquantum limit is realized when both the chemical potential and temperature are less than the energy gap between the lowest and first Landau levels [10,11,30]. Since only chiral branches of the spectrum are occupied, dynamics of these electrons are essentially the same as that of one-dimensional (1D) chiral fermions, where intranode scattering is prohibited [23]. As a result, the effect of the Adler-Bell-Jackiw anomaly becomes enhanced, where the longitudinal current can be relaxed by the internode scattering only. In this ultraquantum limit, the correction term of the longitudinal MC is linearly proportional to B due to 1D chiral dynamics, distinguished from the case of the semiclassical regime [23]. All analysis based on the ultraquantum limit failed to explain our experimental data consistently, indicating that Fermi levels of our samples are located far away from Weyl points [23].

To summarize, in the topological phase transition from a band insulator to a topological insulator in $\text{Bi}_{1-x}\text{Sb}_x$, the upturn behavior above 0.4 T in magnetoconductivity was observed *only* for $B//E$ besides weak antilocalization phenomena near zero magnetic fields ($B < 0.4$ T), which is a fingerprint of the Adler-Bell-Jackiw anomaly. These results are consistent with the Weyl-metal picture and a spectroscopic experiment would be highly desirable to directly measure the peculiar electronic structure of the Weyl metallic state.

This study was supported by Basic Science Research Program and National Nuclear R&D Program through the National Research Foundation of Korea (NRF) funded by the Ministry of Education, Science, and Technology (No. 2010-0021438, No. 2012R1A1B3000550, and No. 2012M2B2A4029488). K.S. appreciates sincere hospitality of APCTP. M.S. wishes to express his thanks to Prof. T. Iwata and K. Tomita for valuable discussions and their support.

*hjkim76@daegu.ac.kr

†tkfd@postech.ac.kr

[1] A. K. Geim and K. S. Novoselov, *Nat. Mater.* **6**, 183 (2007).

- [2] M. E. Peskin and D. V. Schroeder, *An Introduction to Quantum Field Theory* (Addison-Wesley Pub., Seoul, 1997), Chap. 19.
- [3] S. Murakami, *New J. Phys.* **9**, 356 (2007).
- [4] L. Balents, *Physics* **4**, 36 (2011).
- [5] A. A. Burkov and L. Balents, *Phys. Rev. Lett.* **107**, 127205 (2011).
- [6] A. A. Burkov, M. D. Hook, and L. Balents, *Phys. Rev. B* **84**, 235126 (2011).
- [7] G. B. Halász and L. Balents, *Phys. Rev. B* **85**, 035103 (2012).
- [8] S. Adler, *Phys. Rev.* **177**, 2426 (1969).
- [9] J. S. Bell and R. Jackiw, *Nuovo Cimento A* **60**, 4 (1969).
- [10] H. B. Nielsen and M. Ninomiya, *Phys. Lett.* **130B**, 389 (1983).
- [11] D. T. Son and B. Z. Spivak, *Phys. Rev. B* **88**, 104412 (2013).
- [12] L. Fu and C. L. Kane, *Phys. Rev. B* **76**, 045302 (2007).
- [13] J. C. Y. Teo, L. Fu, and C. L. Kane, *Phys. Rev. B* **78**, 045426 (2008).
- [14] H. Guo, K. Sugawara, A. Takayama, S. Souma, T. Sato, N. Satoh, A. Ohnishi, M. Kitaura, M. Sasaki, Q.-K. Xue, and T. Takahashi, *Phys. Rev. B* **83**, 201104(R) (2011).
- [15] T. Koga, J. Nitta, T. Akazaki, and H. Takayanagi, *Phys. Rev. Lett.* **89**, 046801 (2002).
- [16] X. Wu, X. Li, Z. Song, C. Berger, and W. A. de Heer, *Phys. Rev. Lett.* **98**, 136801 (2007).
- [17] F. V. Tikhonenko, A. A. Kozikov, A. K. Savchenko, and R. V. Gorbachev, *Phys. Rev. Lett.* **103**, 226801 (2009).
- [18] J. Chen, H. J. Qin, F. Yang, J. Liu, T. Guan, F. M. Qu, G. H. Zhang, J. R. Shi, X. C. Xie, C. L. Yang, K. H. Wu, Y. Q. Li, and L. Lu, *Phys. Rev. Lett.* **105**, 176602 (2010).
- [19] H.-T. He, G. Wang, T. Zhang, I.-K. Sou, G. K. L. Wong, J.-N. Wang, H.-Z. Lu, S.-Q. Shen, and F.-C. Zhang, *Phys. Rev. Lett.* **106**, 166805 (2011).
- [20] D. J. Bishop, R. C. Dynes, and D. C. Tsui, *Phys. Rev. B* **26**, 773 (1982).
- [21] R. von Helmolt, J. Wecker, B. Holzapfel, L. Schultz, and K. Samwer, *Phys. Rev. Lett.* **71**, 2331 (1993).
- [22] Y.-S. Jho and K.-S. Kim, *Phys. Rev. B* **87**, 205133 (2013).
- [23] See Supplemental Material at <http://link.aps.org/supplemental/10.1103/PhysRevLett.111.246603> for experimental details and theoretical derivations.
- [24] D. Xiao, M.-C. Chang, and Q. Niu, *Rev. Mod. Phys.* **82**, 1959 (2010).
- [25] N. Nagaosa, J. Sinova, S. Onoda, A. H. MacDonald, and N. P. Ong, *Rev. Mod. Phys.* **82**, 1539 (2010).
- [26] N. W. Ashcroft and N. D. Mermin, *State Physics* (Saunders, New York, 1976), Chap. 13.
- [27] A. Kawabata, *J. Phys. Soc. Jpn.* **49**, 628 (1980).
- [28] H.-J. Kim, K.-S. Kim, M. D. Kim, S.-J. Lee, J.-W. Han, A. Ohnishi, M. Kitaura, M. Sasaki, A. Kondo, and K. Kindo, *Phys. Rev. B* **84**, 125144 (2011).
- [29] H.-J. Kim, K.-S. Kim, J.-F. Wang, V. A. Kulbachinskii, K. Ogawa, M. Sasaki, A. Ohnishi, M. Kitaura, Y.-Y. Wu, L. Li, I. Yamamoto, J. Azuma, M. Kamada, and V. Dobrosavljević, *Phys. Rev. Lett.* **110**, 136601 (2013).
- [30] V. Aji, *Phys. Rev. B* **85**, 241101 (2012).